


Optimum transport in systems with time-dependent drive and short-ranged interactionsDeepsikha Das, Punyabrata Pradhan,^{*} and Sakuntala Chatterjee[†]*Physics of Complex Systems, S.N. Bose National Centre for Basic Sciences Block-JD, Sector-III, Salt Lake, Kolkata 700106, India* (Received 13 April 2023; revised 3 July 2023; accepted 14 August 2023; published 7 September 2023)

We consider a one-dimensional lattice gas model of hardcore particles with nearest-neighbor interaction in presence of a time-periodic external potential. We investigate how attractive or repulsive interaction affects particle transport and determine the conditions for optimum transport, i.e., the conditions for which the maximum dc particle current is achieved in the system. We find that the attractive interaction in fact hinders the transport, while the repulsive interaction generally enhances it. The net dc current is a result of the competition between the current induced by the periodic external drive and the diffusive current present in the system. When the diffusive current is negligible, particle transport in the limit of low particle density is optimized for the strongest possible repulsion. But when the particle density is large, very strong repulsion makes particle movement difficult in an overcrowded environment and, in that case, the optimal transport is obtained for somewhat weaker repulsive interaction. Our numerical simulations show reasonable agreement with our mean-field calculations. When the diffusive current is significantly large, the particle transport is still facilitated by repulsive interaction, but the conditions for optimality change. Our numerical simulations show that the optimal transport occurs at the strongest repulsive interaction for large particle density and at a weaker repulsion for small particle density.

DOI: [10.1103/PhysRevE.108.034107](https://doi.org/10.1103/PhysRevE.108.034107)**I. INTRODUCTION**

The ability to manipulate colloidal-particle motion in narrow channels using time-varying optical potential has opened up new research avenues in driven diffusive systems [1–5]. These studies have provided valuable insights into a variety of important aspects of nonequilibrium systems, such as verification and applicability of fluctuation relations, among other things. For example, experiments with colloidal particles driven by an optical trap [6,7] have previously established the validity of a class of fluctuation-dissipation theorem, which predicts entropy production over a finite time interval and that of a generalized Einstein relation [8]. Additionally, the violation of the second law of thermodynamics has also been experimentally demonstrated for small systems over short timescales [9]; see Ref. [10] for review. Recently, a particularly promising research direction that has received a lot of attention is the characterization of particle transport in a periodically driven many-particle system [1,11–13]. These systems find application in a wide range of situations. For example, stochastic pumps [14–17], in which the time-varying external parameters drive the systems away from equilibrium, can thus generate a directed particle flow; also consider the thermal ratchets [18–20], where nonequilibrium fluctuations can induce a directed particle current. Indeed, much attention has been focused on, and significant progress has been made, in understanding the underlying mechanism of directed flow in thermal ratchets and molecular pumps [14].

Notably, the characterization of particle transport in time-varying external potential is important also in the context

of driven fluids in confined geometry, leading to the identification of a number of unexpected consequences, such as negative differential resistance and absolute negative mobility among others [12,13,21–26]. In the past, particle transport in colloidal suspensions in narrow channels have motivated studies of noninteracting particles, driven by a moving potential barrier, using dynamic density functional theory [12,13]. Eventually, several many-particle models were also put forth in an effort to theoretically understand the role of hardcore interactions in these systems [27]. One particularly important question here is whether the system can support a nonzero dc (time-averaged) current when it is driven by a time-periodic driving force. Although the presence of an external forcing would typically suggest the presence of a current in the system, the periodic nature of the driving, however, means that the net force acting on the system over a time period is zero. In that case, do such systems still carry a dc current? If so, then in what direction does the current flow? Another intriguing question is whether it is possible to optimize the particle current by tuning various control parameters.

In order to address the above questions, a series of works [27–29] considered the paradigmatic models of simple exclusion processes [30], in which the interaction among the particles was assumed to be of the simplest possible form, i.e., of hardcore exclusion. The motion of the particles were described on a lattice where particles hop from one site to a neighboring unoccupied site; in that case, the periodic external potential was simply represented by space- and time-dependent hopping rates. Depending on whether the time-varying hopping rates were present only on particular sites or were present throughout the system, it was shown through numerical simulations and a perturbative approach that the dc current flowing through such a system could either vanish (inversely with system size) or have a finite value.

^{*}punyabrata.pradhan@bose.res.in[†]sakuntala.chatterjee@bose.res.in

Furthermore, the dc current was found to exhibit nonmonotonic dependence on the time period of the drive. Several interesting features such as current reversal and system-size-dependent transport were observed [29] in the case when time-varying potential maintains a position-dependent phase relation among sites that results in a nonzero dc current.

Subsequently, in another study of a many-particle lattice model [31], our group developed a new simple method of modeling a periodically moving drive in a system of hardcore particles diffusing on a one-dimensional ring. Motivated by experiments where particle movements are controlled by moving optical potential, we studied a system with an on-site potential that moves along the ring with velocity v , spending a residence time $1/v$ at each site. Such a localized δ potential, that was termed as a “defect,” modifies the particle transition rates at its current position. For simplicity, we considered a delta potential with a positive strength, corresponding to a strongly localized infinite potential barrier. Using numerical simulation and a mean-field theory, we observed that, in the time-periodic steady state, a density inhomogeneity is created around the defect, resulting in a dc current that scales as $1/L$ with system size L . The direction and magnitude of the dc current was controlled by tuning the defect velocity, particle density, and the bulk diffusivity of particles. Moreover, in the presence of multiple defect sites [32], an interesting collective behavior was observed when the defect sites were close enough so that their respective density patterns generated by each of the defects overlap with each other. Interestingly, reversal of current has also been observed in a slightly different setup [33] in the context of a single particle, which diffuses in a two-dimensional channel of varying width and is driven by a force having a random orientation across the channel; in this case, the current reversal happens by tuning both the transverse and the longitudinal drive.

So far, in the above-mentioned studies of many-particle lattice models in the presence of time-varying drive, the type of interaction considered between the particles was simply hardcore exclusion. However, in real systems, particles can also experience short-ranged attraction or repulsion and the interplay between external drive and interparticle interactions are expected to give rise to nontrivial effects. In order to investigate this scenario, in the present work we consider paradigmatic Ising-like lattice gases on a ring of L sites, where hardcore particles diffuse and interact via nearest-neighbor attractive or repulsive potential. In other words, in addition to the hardcore exclusion, a particle, in the case of repulsive (attractive) interaction, now prefers to have its neighboring site empty (occupied). Here we are primarily interested in exploring how the strength of the interaction potential affects the particle current in the system. Does the system still support current reversal? Is there an optimum interaction strength for which magnitude of the current in either direction is largest?

In this paper, by performing Monte Carlo simulations and analytical calculations within mean-field theory, we demonstrate that the system does, in fact, support a dc current in such scenario. We characterize how attractive or repulsive interaction among the particles affect the transport and determine the conditions for achieving optimal transport in the system. We show that a moving defect (a “delta” potential

barrier) always induces current in the negative direction, i.e., along the direction opposite to the defect movement. But, due to the density inhomogeneity produced by the defect movement, the diffusive current in the system flows in the positive direction. As a result, when the bulk diffusion in the system is negligibly small, we find current in the negative direction. However, as the bulk diffusion becomes stronger, the current changes sign and becomes positive. By varying the interaction strength, particle density and the defect velocity, we determine the parameter regime that yields the optimum current in the system in either direction.

It turns out that an attractive interaction among the particles hinders transport, while a repulsive interaction enhances it. For negligible diffusion, the current in the limit of low particle density is maximized for the strongest possible repulsive strength. However, when the density is high, very strong repulsion blocks certain transitions in the overcrowded system and optimal current is obtained for a relatively weaker repulsion. Our analytical calculations based on mean-field theory support these conclusions and qualitatively explain our simulation data. For finite diffusive current, we have not been able to perform analytical calculations. Our simulations for this case show that the interplay between defect-induced current and diffusive current changes the optimality conditions significantly. For large particle density, defect induced current wins over the diffusive current, which makes the net current negative. We find strongest repulsion is most suitable for optimal transport in this regime. For small density, diffusive current dominates and the net current is positive. Our simulations show a weaker repulsive interaction maximizes this current.

The organization of the paper is as follows: We describe the model in Sec. II. In Sec. III, we describe the simplest possible case, where dynamics in the bulk of the system is absent (i.e., when the barrier velocity is sufficiently larger than the rate of bulk diffusion). Analytical formalism corresponding to that case is presented in Secs. III A and III B while the results are shown and discussed in Sec. III C. In Sec. IV, we discuss the case when bulk dynamics can be compared to the other rates in the system. Our conclusions are presented in Sec. V.

II. THE MODEL

We consider paradigmatic Ising-like [34] lattice gases consisting of hardcore particles, which diffuse on a ring of L sites and interact through nearest-neighbor pair potentials. In the absence of any drive (i.e., corresponding to equilibrium), the system is governed by standard stochastic Kawasaki dynamics. The drive is applied through an external potential barrier, which moves periodically on the ring, and it essentially modifies the local particle hopping rates, satisfying a local detailed balance condition [35]. As a result, the transition or particle hop rates, unlike in equilibrium, are now time dependent. More specifically, we incorporate such a time-dependent drive by introducing “defect” sites, where a delta potential barrier is present. The rest of the sites in the system are called bulk sites. Consequently the particle hopping rates at the “defect” sites will differ from the bulk sites. Each defect resides at a site for a time duration $\tau = 1/v$, before moving to the right [31,32]. The model is shown in Fig. 1. The energy function

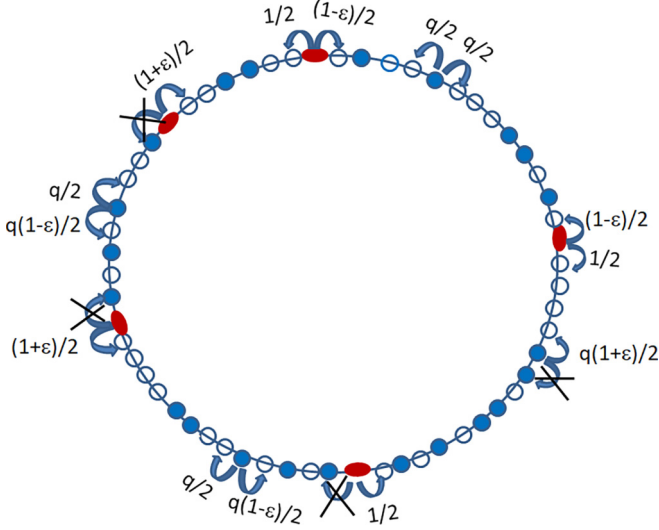


FIG. 1. Schematic diagram of the model. Red solid ellipses represent occupied defect sites while the blue solid (empty) circles are occupied (empty) bulk sites. A particle can jump to one of its neighboring site provided the destination site is empty. The transition rates depend on the local configurations around the departure site, as specified in Eq. (3).

for the system can be written as

$$H = -\frac{K}{2} \sum_{i,j} \eta_i^{\{\alpha_k\}} \eta_j^{\{\alpha_k\}} + \sum_i \eta_i^{\{\alpha_k\}} V_i, \quad (1)$$

where $\eta_i^{\{\alpha_k\}}$, taking value 0 or 1, denotes occupancy of site i and $-\infty < K < \infty$ is the interaction strength; here the indices $\{\alpha_k\} \equiv \{\alpha_1, \alpha_2, \dots, \alpha_N\}$ are a set of N elements with the k th element, α_k , being the position of the k th defect and $\langle i, j \rangle$ denotes that sites i and j are the nearest-neighbor ones. The quantity $V_i = \sum_k V_0 \delta_{i, \alpha_k}$ is the external potential at site i with V_0 representing the height of the onsite potential barrier. It is convenient to map from the interaction strength K to an equivalent dimensionless parameter ϵ [36] through the following relation,

$$e^{-\beta K} = \frac{(1 + \epsilon)}{(1 - \epsilon)}, \quad (2)$$

where $|\epsilon| \leq 1$ as $0 \leq e^{-\beta K} < \infty$, with β being the inverse temperature. Note that the case with $\epsilon > 0$, $\epsilon < 0$, and $\epsilon = 0$ correspond to repulsive, attractive, and simply hardcore interactions, respectively. Depending on the local transition rate, a particle can move to its immediate left (right) site provided that the site is empty. Such transitions can happen in four possible ways and corresponding rates for leftward and rightward transitions can be as follows:

$$\begin{array}{ll} 0010 \xrightleftharpoons[c(1-\epsilon)]{c} 0100 & 0100 \xrightleftharpoons[c(1-\epsilon)]{c} 0010 \\ 1010 \xrightleftharpoons[c(1+\epsilon)e^{-\beta V_i}]{} 1100 & 0101 \xrightleftharpoons[c(1+\epsilon)]{} 0011 \\ 0011 \xrightleftharpoons[c(1-\epsilon)e^{-\beta V_i}]{} 0101 & 1100 \xrightleftharpoons[c(1-\epsilon)]{} 1010 \\ 1011 \xrightleftharpoons[ce^{-\beta V_i}]{} 1101 & 1101 \xrightleftharpoons[ce^{-\beta V_i}]{} 1011, \end{array} \quad (3)$$

where $c = 1/2$ or $q/2$ if the departure site is a defect site or a bulk site, respectively. Indeed, for defect velocity $v = 0$, the transition rates satisfy detailed balance condition and, in that case, the system in the long-time limit is governed by the equilibrium Boltzmann-Gibbs distribution with respect to the energy function given in Eq. (1). For simplicity, in this study, we have considered a single moving defect, which represents an infinite (delta) potential barrier with $V_0 = \infty$, periodically moving over the ring with velocity v ; consequently, no particle can enter the defect site.

III. $q = 0$: NO DYNAMICS IN THE BULK

A. Analytical formalism for a periodically moving defect

In this section, we develop an exact theoretical framework to deal with the simplest (but, still driven and thus nontrivial) case when the inverse hopping rate is much larger compared to the typical residence timescale of the defect. That is, we assume the bulk hopping rate $q = 0$, implying the dynamics in the bulk is completely frozen. In that case, a particle can hop during an infinitesimal time interval dt only if its position coincides with the position of the defect denoted by α . Starting from an initial configuration, the system eventually reaches a time-periodic steady state, given that sufficient time has passed. The density profile of the system has a form of a traveling wave moving over the lattice with the same velocity v as that of the moving defect. The defect spends time τ at a particular site before moving on to the next site, where $\tau = 1/v$ is the residence time of the defect. When the defect spends one Monte Carlo step on each lattice site, v is measured as 1. We have measured density profile at time steps $t = n\tau$ just before the defect moves on to the next site, after spending time τ at the previous site, with $n = 0, 1, 2, \dots, \infty$. Therefore we can write the discrete time evolution equation [31] for density $\rho_i^{(\alpha)}(t) = \langle \eta_i^{(\alpha)}(t) \rangle$ as

$$\langle \rho^{(\alpha+1)}(t + \tau) | = \langle \rho^{(\alpha)}(t) | W^{(\alpha+1)}, \quad (4)$$

where $\langle \rho^{(\alpha)}(t) | \equiv \{\rho_1^{(\alpha)}(t), \dots, \rho_i^{(\alpha)}(t), \dots, \rho_L^{(\alpha)}(t)\}$ is a row vector of length L , with i th element being $\rho_i^{(\alpha)}(t)$ and α denoting the position of the defect. The operator $W^{(\alpha+1)}$ is the transition matrix when the defect site is located at $\alpha + 1$, i.e., its structure, (explicitly shown in Appendix A), depends on the position of the defect site. Elements of $W^{(\alpha+1)}$ involve $a_+(a_-)$, the conditional probabilities that, given the defect site is occupied, a particle from the defect site moves to its unoccupied right (left) neighboring site during the residence time τ . Starting from microscopic dynamics, we can have their expressions as follows:

$$a_+ = \sum_{m=1}^6 C_m^+ \omega_m^+, \quad a_- = \sum_{n=1}^6 C_n^- \omega_n^-, \quad (5)$$

where C_m^+ , C_n^- are the conditional probabilities of different local configurations favorable for right and left hopping respectively during the residence time τ , given the defect site is occupied. The quantities ω_m^+ and ω_n^- denote the transition probabilities for right and left hopping, respectively, from an

occupied defect site during time τ . For example, we can write the conditional probabilities,

$$\begin{aligned} \mathcal{C}_1^+ &= \text{P}(00\hat{1}01|\eta_{\alpha+1}^{(\alpha)} = 1) \\ &= \frac{\langle [1 - \eta_{\alpha-1}^{(\alpha)}][1 - \eta_{\alpha}^{(\alpha)}]\eta_{\alpha+1}^{(\alpha)}[1 - \eta_{\alpha+2}^{(\alpha)}]\eta_{\alpha+3}^{(\alpha)} \rangle}{\langle \eta_{\alpha+1}^{(\alpha)} \rangle}, \end{aligned} \quad (6)$$

$$\begin{aligned} \mathcal{C}_1^- &= \text{P}(10\hat{1}00|\eta_{\alpha+1}^{(\alpha)} = 1) \\ &= \frac{\langle \eta_{\alpha-1}^{(\alpha)}[1 - \eta_{\alpha}^{(\alpha)}]\eta_{\alpha+1}^{(\alpha)}[1 - \eta_{\alpha+2}^{(\alpha)}][1 - \eta_{\alpha+3}^{(\alpha)}] \rangle}{\langle \eta_{\alpha+1}^{(\alpha)} \rangle}, \end{aligned} \quad (7)$$

and the corresponding transition rates,

$$\omega_1^+ = \omega_1^- = \frac{1 - \epsilon}{2 - \epsilon} \left[1 - e^{-(2-\epsilon)/4v} \right], \quad (8)$$

where \mathcal{C}_1^+ and \mathcal{C}_1^- represent the conditional probabilities for local configurations $00\hat{1}01$ and $10\hat{1}00$, respectively, given that the defect site is occupied. In that case, the quantities ω_1^+ and ω_1^- denote the transition probabilities corresponding to configuration $00\hat{1}01$ and $10\hat{1}00$, respectively, during the residence time τ with $\hat{1}(\hat{0})$ denoting an occupied (unoccupied) defect site (see Appendix B for details). Due to the time-periodic structure of the steady state, the density profile comes back to itself each time the defect moves across the ring and completes a cycle. So the time-evolution operator $W^{(\alpha+1)} \dots W^{(L)} W^{(1)} \dots W^{(\alpha-1)} W^{(\alpha)}$ over a full time period must have an eigenvector $\langle \rho_{\text{st}}^{(\alpha)} |$ with eigenvalue unity. Then the steady-state density at i th site satisfies the following condition:

$$\rho_{\text{st},i}^{(\alpha+1)} = \rho_{\text{st},i-1}^{(\alpha)}, \quad (9)$$

which follows from the time-periodic structure of the steady-state density and from Eq. (4). To solve for the density profile in a time-periodic steady state, we find that, at the time of measurement, the defect site α registers lower density compared to the bulk as particles cannot hop into the defect site. Rather they can only hop out of the defect site. For $q = 0$ the neighboring sites ($\alpha \pm 1$) can only receive particles from the defect site without any loss. The site ($\alpha + 1$) thus has a higher density compared to that at the bulk. On the other hand, the site ($\alpha - 1$) which was previously occupied by the defect and has already registered lower density could only receive particle from the defect site α and its density goes back to the bulk level. Therefore regarding the structure of the density profile as a function of position, an ansatz [31] can be written in the form of a traveling density wave, which moves with the defect α . That is, we have

$$\begin{aligned} \rho_{\text{st},i}^{(\alpha)} &= \rho_- \quad \text{for } i = \alpha \\ \rho_{\text{st},i}^{(\alpha)} &= \rho_+ \quad \text{for } i = \alpha + 1 \\ \rho_{\text{st},i}^{(\alpha)} &= \rho \quad \text{otherwise.} \end{aligned} \quad (10)$$

The above ansatz can be now used in Eqs. (4) and (9) to obtain the following condition:

$$\rho_+ a_- + \rho_- = \rho_b, \quad (11)$$

$$\rho_+ a_+ + \rho_b = \rho_+, \quad (12)$$

where ρ_b is the bulk density. The above set of equations can be readily solved by using particle-number conservation

condition $\rho_+ + \rho_- + (L - 2)\rho_b = L\rho$, and we obtain the exact densities,

$$\rho_b = \frac{(1 - a_+)L}{2 - a_+ - a_- + (1 - a_+)(L - 2)} \rho \simeq \rho, \quad (13)$$

$$\rho_+ \simeq \frac{1}{1 - a_+} \rho, \quad (14)$$

$$\rho_- \simeq \frac{1 - a_+ - a_-}{1 - a_+} \rho, \quad (15)$$

in the limit of large system size ($L \gg 1$). Then, from Eqs. (14) and (15), it is evident that $\rho_+ > \rho$ and $\rho_- < \rho$, i.e., a peak and a trough are formed in front of and at the defect site, respectively.

Indeed, size of the trough and the peak formed around the defect site are different, thus resulting in a nonzero particle current in the system as explained below. Note that, for $q = 0$, the contribution to the net particle current comes from only the two bonds adjacent to the defect site as no hopping takes place across any other bonds in the system. Thus in this case, the particle current consists of two components J_+ and J_- , defined to be the time rate of rightward and leftward movement of particles, respectively, from the defect site. The total current is then simply the algebraic sum of them. As the defect visits a particular site with rate v/L , the expression for the dc particle current can be written as

$$J = J_+ + J_- = \frac{v}{L} [\langle \eta_{\alpha+1}^{(\alpha)} \rangle a_+ - \langle \eta_{\alpha+1}^{(\alpha)} \rangle a_-], \quad (16)$$

which can be written in terms of ρ_{\pm} from Eq. (14) and (15) as

$$J = \frac{v}{L} [(\rho_+ - \rho) + (\rho_- - \rho)] = \frac{v}{L} (\rho_+ + \rho_- - 2\rho), \quad (17)$$

where the positive and negative contributions to the net current is given by

$$J_+ = \frac{v}{L} [\langle \eta_{\alpha+1}^{(\alpha)} \rangle a_+] = \frac{v}{L} (\rho_+ - \rho), \quad (18)$$

and

$$J_- = -\frac{v}{L} \langle \eta_{\alpha+1}^{(\alpha)} \rangle a_- = \frac{v}{L} (\rho_- - \rho), \quad (19)$$

respectively.

B. Mean-field theory

The exact expressions for the conditional probabilities a_+ and a_- are given in Eq. (5) [for details, see Eqs. (B1) to (B17) in Appendix B]. However, we note that these conditional probabilities involve calculations of multipoint correlation functions, which are difficult to obtain exactly. Therefore, to write a_+ and a_- as explicit functions of the system parameters ϵ , ρ , and v , we proceed further by resorting to mean-field approximations, where multipoint correlations \mathcal{C}_m^+ and \mathcal{C}_n^- (where $m, n = 1, 2, \dots, 6$) are simply assumed to be factorized and we thus have the following expressions of the above-mentioned quantities:

$$\mathcal{C}_1^+ = \mathcal{C}_1^- = \rho(1 - \rho_-)(1 - \rho)^2, \quad (20)$$

etc., and

$$a_+ = (1 - \rho)[(1 - \rho)(1 - \rho_-)\rho\omega_1^+ + \rho^2(1 - \rho_-)\omega_2^+ + (1 - \rho)^2(1 - \rho_-)\omega_3^+ + \rho(1 - \rho_-)(1 - \rho)\omega_4^+ + \rho_-(1 - \rho)\omega_5^+ + \rho_-\rho\omega_6^+] \quad (21)$$

and

$$a_- = (1 - \rho_-)[\rho(1 - \rho)^2\omega_1^- + \rho^2(1 - \rho)\omega_2^- + (1 - \rho)^3\omega_3^- + \rho(1 - \rho)^2\omega_4^- + \rho(1 - \rho)\omega_5^- + \rho^2\omega_6^-]. \quad (22)$$

Now by combining Eqs. (14) and (15), we have the following equation:

$$(\rho_- - \rho)(1 - a_+) + a_-\rho = 0, \quad (23)$$

which should now be solved as a function of the parameters ϵ , ρ , and v . Indeed, if expressions for a_+ and a_- from Eqs. (21) and (22) are substituted into Eq. (23), then we obtain the following quadratic equation for ρ_- :

$$(\rho_- - \rho)[1 - (1 - \rho)\{(1 - \rho)(1 - \rho_-)\rho\omega_1^+ + \rho^2(1 - \rho_-)\omega_2^+ + (1 - \rho)^2(1 - \rho_-)\omega_3^+ + \rho(1 - \rho_-)(1 - \rho)\omega_4^+ + \rho_-(1 - \rho)\omega_5^+ + \rho_-\rho\omega_6^+\}] + \rho(1 - \rho_-)[\rho(1 - \rho)^2\omega_1^- + \rho^2(1 - \rho)\omega_2^- + (1 - \rho)^3\omega_3^- + \rho(1 - \rho)^2\omega_4^- + \rho(1 - \rho)\omega_5^- + \rho^2\omega_6^-] = 0. \quad (24)$$

The explicit analytic solution of the above quadratic equation is quite cumbersome and we therefore numerically solve it using *Mathematica*, where we retain only the physically acceptable root (i.e., not larger than unity), leading to a numerical solution of ρ_+ and ρ_- . Consequently, the mean-field expression for the particle current can be obtained using Eqs. (21) and (22) [also see Eqs. (B1) to (B17) in Appendix B for details] as follows:

$$J = \frac{v}{L}\rho_+(\rho_- - \rho)\{(1 - \rho)[1 - e^{-(1+\epsilon)/4v}] + \rho(1 - e^{-1/4v})\}. \quad (25)$$

In the limit of small and large ρ , the solutions for ρ_{\pm} , and hence for particle current J , however, take simple forms as we write a_{\pm} in the leading order of ρ and $(1 - \rho)$, respectively. For small ρ , we retain leading order terms in ρ in its functions and we immediately obtain

$$a_+ \approx \rho_-[\rho(3\omega_3 - \omega_1 - \omega_4 - 2\omega_5 + \omega_6) - (\omega_3 - \omega_5)] + \rho(\omega_1 - 3\omega_3 + \omega_4) + \omega_3 \quad (26)$$

and

$$a_- \approx \rho_-[\rho(3\omega_3 - \omega_1 - \omega_4 - \omega_5) - \omega_3] + \rho(\omega_1 - 3\omega_3 + \omega_4 + \omega_5) + \omega_3. \quad (27)$$

Substituting Eqs. (26) and (27) into Eq. (23), we have trough density,

$$\rho_- = \frac{1 - 2\omega_3}{1 - \omega_3}\rho \quad (28)$$

and

$$\rho_+ = \frac{\rho}{1 - \omega_3}. \quad (29)$$

Now the scaled current JL can be straightforwardly written as

$$JL = \frac{v\omega_5(1 - 2\omega_3)\rho^2}{(1 - \omega_3)^2}, \quad (30)$$

which is interestingly quadratic in ρ . On the other hand, for large ρ , we retain terms in leading order of $(1 - \rho)$ and thus obtain

$$a_+ \approx \omega_6(1 - \rho) + (\omega_2 - \omega_6)(1 - \rho)(1 - \rho_-) \quad (31)$$

and

$$a_- \approx \omega_6(1 - \rho_-) + (\omega_2 + \omega_5 - 2\omega_6)(1 - \rho)(1 - \rho_-). \quad (32)$$

Finally substituting Eqs. (31) and (32) into Eq. (23), we have the trough density

$$\rho_- = 1 - \frac{(1 - 2\omega_2 - 2\omega_5 + 3\omega_6)}{(1 - \omega_2 - \omega_5 + \omega_6)^2}(1 - \rho), \quad (33)$$

the peak density

$$\rho_+ = 1 - (1 - \omega_6)(1 - \rho), \quad (34)$$

and consequently the scaled particle current can be written as

$$JL = \frac{v\omega_6}{\omega_6 - 1}(1 - \rho), \quad (35)$$

which are in fact linear in $(1 - \rho)$.

C. Simulation results and comparison with mean-field theory

In this section, we present results obtained from simulations and then we compare them with analytical results from mean-field theory. We have used system size $L = 512$ throughout. As predicted by our analytical formalism developed in Sec. III A, we indeed find a density peak and a density trough around the defect site. Since we are primarily interested to know the effect of interparticle interaction on the system, first we study variation of size of the density peak $\rho_+ - \rho$ and size of the density trough $\rho - \rho_-$ against interaction strength ϵ . The system often behaves differently for small and large values of bulk density. So, we have shown data for both of the cases. Then the variation of the net particle current J is studied against interaction strength ϵ , bulk density ρ , and defect velocity v . For small or moderate values of bulk hopping rate q , we find that magnitude of the particle current is maximum around $v \simeq 0.16$ and this particular value is not too sensitive on the choice of ρ or ϵ . Since we are interested in optimum particle transport, we perform most of our measurements at this particular v value only, unless explicitly mentioned otherwise.

In Fig. 2, we plot the size of density peak $\rho_+ - \rho$ and that of density trough $\rho - \rho_-$ as a function of the interaction strength ϵ . We find that, as ϵ increases from negative to positive values, the density differences $(\rho_+ - \rho)$ and $(\rho - \rho_-)$ also increase. The variation in both these quantities against ϵ are interestingly nonmonotonic with a peak at moderately large positive ϵ values. Our mean-field calculation also captures this nonmonotonic behavior but does not provide good quantitative agreement with the simulation data.

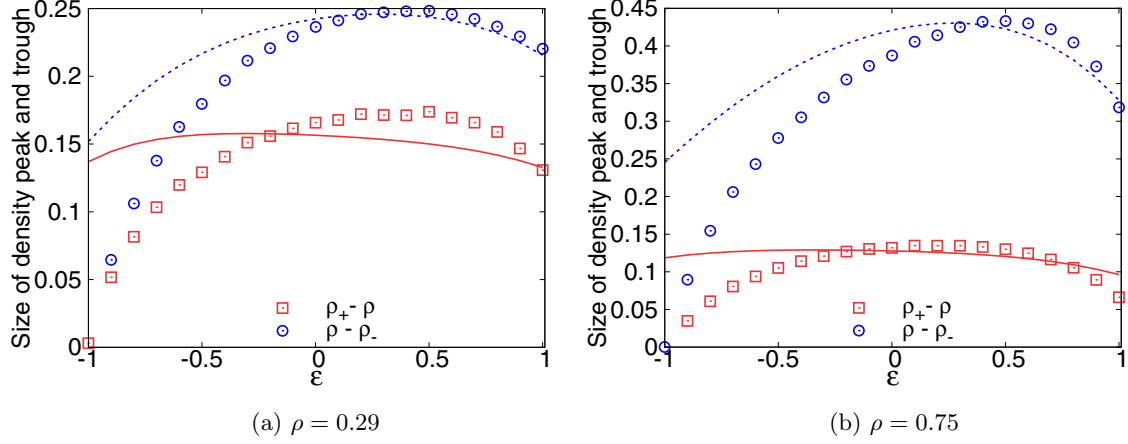


FIG. 2. Size of the density peak and trough, $(\rho_+ - \rho)$ and $(\rho - \rho_-)$ are plotted against ϵ in panels (a) and (b). Mean-field results are presented by solid and dotted lines, respectively. It is evident from both the panels that depth of the trough is always greater than height of the peak. Nonmonotonic variation against ϵ can be seen in both the quantities which is more pronounced for $(\rho - \rho_-)$ with a maximum at a large positive ϵ . Mean-field theory can qualitatively capture such behavior in the repulsive region, while it fails in the region of attractive interaction. Points, simulations; lines, mean-field theory.

Now, in the remaining part of this subsection, we show the variation of particle current as a function of various system parameters, emphasizing on how such variations are affected by the interaction strengths. To be concise, in Table I, we list the parameter values we have used in our study and include a brief discussion justifying our choices. In our study of particle current J as a function of ϵ , we find qualitatively different nature of variations at small and large ρ . To show this effect, we present J vs ϵ data for five different ρ , spanning from low to high values (see Table I). As we discuss in details below, the J vs ρ characteristic curve shows a dramatic dependence on the interaction strength. To highlight this aspect, we show data for a wide range of ϵ , starting from strong attraction to strong repulsion; the corresponding values are listed in Table I. For J vs v characteristics, we separately show how the curve changes with ϵ for low- and high-density cases, since the mechanism of optimum transport is different in these two cases. We have used one representative values of ϵ for attractive, noninteracting, repulsive cases each, and also $\epsilon = 1$, the case for the strongest repulsion, which is quite relevant for optimal transport.

In Fig. 3, the variation of scaled particle current JL with ϵ has been shown for different ρ values. At $\epsilon = -1$, because of strong attractive interaction among the particles, the sys-

tem supports one single cluster, containing all the particles. Therefore, quite expectedly, the particle current vanishes in this particular limit. As ϵ increases, a density profile consisting of a peak and a trough as shown in Fig. 12 is formed around the defect site and consequently the current becomes nonzero. As ϵ increases further, the density peak and trough become more pronounced (as shown in Fig. 2), thus resulting in larger current magnitude. However, for positive ϵ , current shows qualitatively different behavior for small and large ρ . For small ρ values, the current remains almost constant over a large range of ϵ before showing a rather mild increase near $\epsilon = 1$.

This behavior can be explained from our data in Fig. 2(a), where the difference between the two curves (red square and blue diamond), which represent the asymmetry between the sizes of density peak and trough, remains unchanged for a

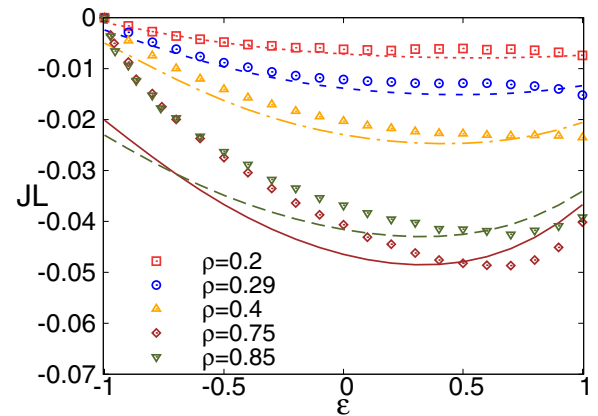


FIG. 3. Scaled current are plotted against epsilon along with mean-field results (presented by dotted line ($\rho = 0.2$), short-dashed line ($\rho = 0.29$), dot-dashed line ($\rho = 0.4$), solid line ($\rho = 0.75$), and dashed line ($\rho = 0.85$)). Current vanishes at $\epsilon = -1$ and remains negative elsewhere. For small and intermediate ρ current is largest for $\epsilon = 1$, while for large ρ it shows a peak at a slightly smaller ϵ value.

TABLE I. Parameter values used for the studies of current variation.

J vs ϵ		J vs ρ		J vs v	
ρ	v	ϵ	v	ϵ	ρ
0.2		-0.9			
0.29		-0.5		-0.6	
0.4	0.16	0	0.16	0	0.29
0.75		0.5		0.6	0.75
0.85		0.97		1	

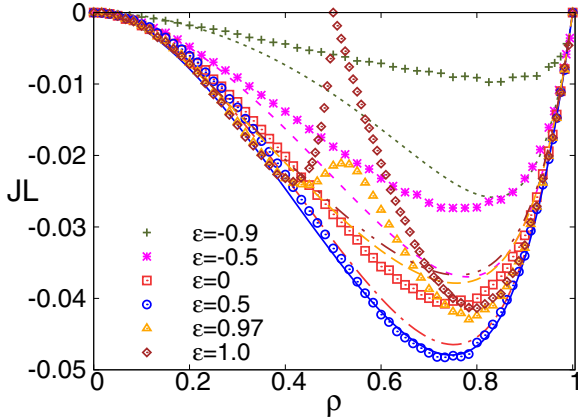


FIG. 4. Scaled current vs density for various interaction strengths. Discrete points show simulation data and lines show mean-field calculations. We have used dotted ($\epsilon = -0.9$), short-dashed ($\epsilon = -0.5$), dashed ($\epsilon = 0$), solid ($\epsilon = 0.5$), dot-dashed ($\epsilon = 0.97$), and a dot-dot-dashed line ($\epsilon = 1$). For all epsilon values, current shows nonmonotonic variation with density. For attractive interaction and moderate repulsive interaction, current shows a single peak at a density $> 1/2$. However, as repulsion becomes stronger, current shows two peaks, separated by a minimum at $\rho = 1/2$. Although mean-field theory fails to capture the double peak, we offer an alternative simple explanation in the text.

significant range of positive ϵ but increases when ϵ is close to 1. Note that this asymmetry is directly related to the current as shown in Eq. (17). For large ρ , on the other hand, the current shows a peak at $\epsilon \simeq 0.7$ and then gradually decreases beyond that. This behavior is consistent with our simulation data presented in Fig. 2(b), where the two curves are seen farthest apart at that particular ϵ . Note that the mean-field theory can qualitatively capture the peak current for large ρ , but, for small ρ , it is unable to reproduce the upswing shown by our data near $\epsilon = 1$. We find similar disagreement in Fig. 2(a) as well where mean-field theory does not quite capture the variation of the peak size.

In Fig. 4, we plot the scaled current JL as a function of bulk density ρ for various ϵ values. In the dilute $\rho \rightarrow 0$ and dense $\rho \rightarrow 1$ limits, the particle current vanishes for all ϵ as expected. We have been able to analytically show [see Eqs. (30) and (35)] that, in the small density limit, the current $\sim \rho^2$ varies quadratically with ρ , while, in the large-density limit, the current $\sim (1 - \rho)$ is, however, linear. This limiting behavior agree quite well with the simulation data. We observe that for an intermediate density ρ^* , the particle current shows a maximum. However, when ϵ takes large negative value, the overall magnitude of the current becomes vanishingly small because of the strong attractive interaction among the particles, enhancing cluster formation that leads to decrease in particle mobility. As the particle attraction weakens, the current also increases and the peak at ρ^* gets higher. Our mean-field results successfully capture this trend, although ρ^* from mean-field shows dependence on ϵ unlike a nearly constant $\rho^* \simeq 0.75$ obtained from numerics for all ϵ . As ϵ changes sign and becomes positive, the repulsive interaction does not favor successive occupied sites, thus giving rise to a special point at $\rho = 0.5$ and $\epsilon = 1$ when the only allowed

configuration is that with the alternate sites occupied by particles. No transitions are possible from this configuration and hence the current vanishes. This is verified from simulations where the current sharply becomes zero at $\rho = 0.5$ for $\epsilon = 1$. Thus the nearest-neighbor exclusion generates another peak in the current at a somewhat lower density value $\rho < 0.5$. However, even as ϵ falls slightly below unity, this effect weakens and the zero of current at half-filled density is replaced by a mild minimum. Our mean-field calculations are unable to capture this particular effect induced by strong nearest-neighbor repulsion and simply predicts a single peak for current for all ϵ ; notably the mean-field theory shows good agreement with the numerical data for moderate repulsive interaction strengths.

In Fig. 5, we depict variation of current with defect velocity v for different interaction strengths and two different ρ values.

In all cases, the limit $v \rightarrow 0$ corresponds to the equilibrium case when the current vanishes which is expected. For very large v , the defect movement becomes too fast for the particles to respond and the current vanishes here, too. An intermediate v therefore maximizes the current which can be seen both from simulation data and mean-field calculations. As ϵ increases from negative to positive values, the peak current increases monotonically for $\rho = 0.29$ [Fig. 5(a)], while, for $\rho = 0.75$, the peak current shows a nonmonotonic variation for positive ϵ [Fig. 5(b)]. This is indeed consistent with the variation observed in Fig. 3.

In Figs. 3–5, we plot current as a function of one of the three variables ϵ , ρ , and v , keeping the other two constant. To understand the condition of optimum transport, we need to identify how ρ , ϵ , and v should be chosen such that the current in the system is maximized. To this end, in Fig. 6, we present heat-maps, where we simultaneously vary ϵ and v for a fixed ρ . Our simulation data are presented in Figs. 6(a) and 6(b) and our mean-field calculations appear in Figs. 6(c) and 6(d).

These plots clearly demonstrate that the repulsive interaction in fact facilitates particle transport in the system. For smaller density, current always increases as ϵ increases and, quite interestingly, largest current is obtained at $\epsilon = 1$ (nearest-neighbor exclusion), when the repulsion is strongest. For larger density, on the other hand, very strong repulsion makes certain transitions energetically unfavorable. This hinders particle transport. Therefore, in this case, optimum current is obtained at an intermediate ϵ value. Our mean-field calculations manage to correctly reproduce this optimality as seen in Fig. 6(d), but they do not work so well as seen in Fig. 6(c). Note that the scale used to present the current for low density is widely different from that in the high density. This means that, when the density is low, for a particular density optimum transport can be achieved, but the magnitude of the current is far smaller than that obtained in the optimum regime at high density. This is seen more clearly in Fig. 7.

In Fig. 7, we depict through the heat-maps the variation of particle current when ϵ and ρ are varied by keeping v constant. Apart from the usual choice of $v = 0.16$, here we have also presented data for $v = 1$. These plots show that, to obtain the optimum transport, ρ needs to be sufficiently high. Since, in the high density regime, an intermediate strength of repulsive interaction gives the maximum current, the optimum transport happens away from $\epsilon = 1$. Note that, even in this figure, the

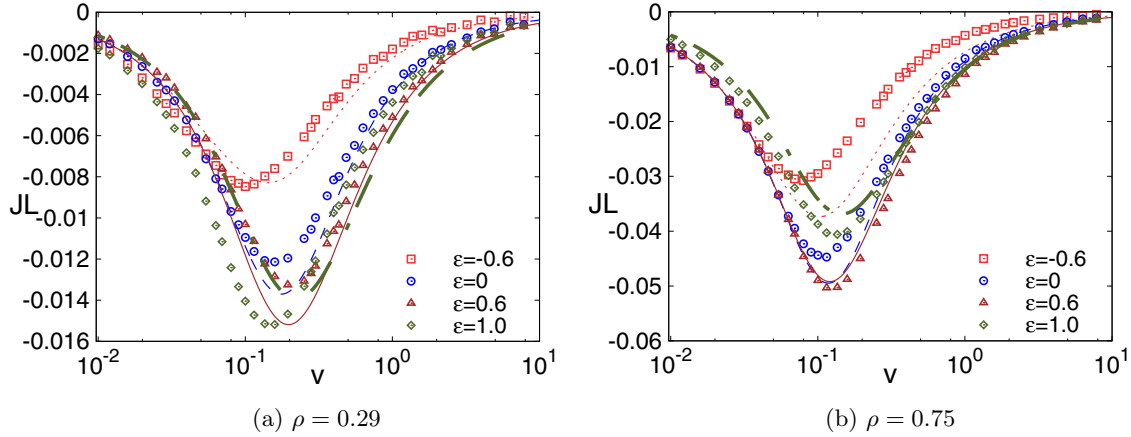


FIG. 5. Scaled current JL plotted against defect velocity v along with mean-field results (represented by dotted ($\epsilon = -0.6$), short-dashed ($\epsilon = 0$), solid ($\epsilon = 0.6$), and dot-dashed line ($\epsilon = 1$)) in panels (a) and (b). Current vanishes in the small v and large v limit and shows a peak in between. The peak height increases as interaction changes from attraction to repulsion. Largest peak is obtained for a large positive value of ϵ . Mean-field theory explains the numerical data qualitatively.

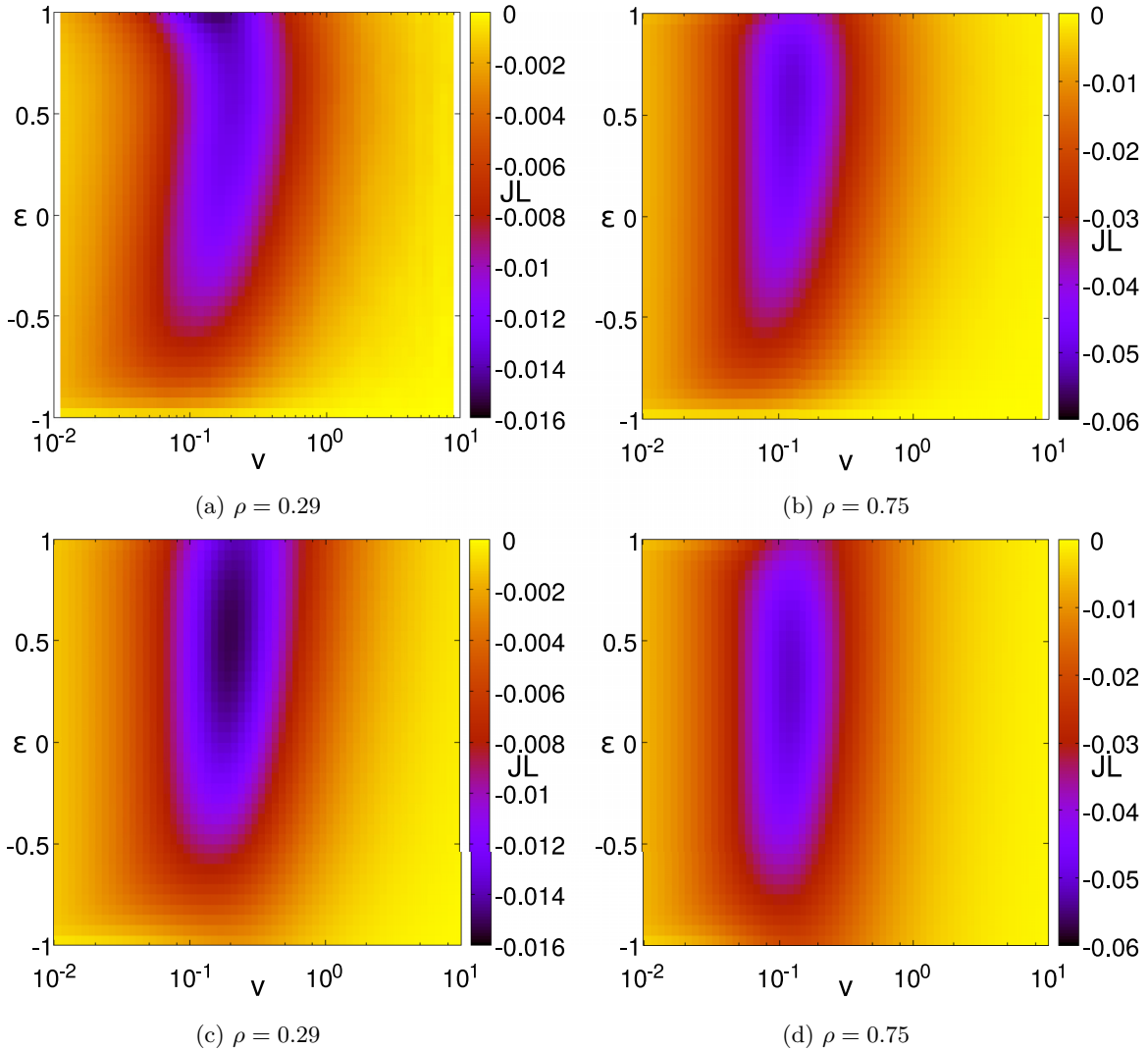


FIG. 6. Scaled particle current JL is plotted against ϵ and v . Panels (a) and (b) represent numerical data while panels (c) and (d) show mean-field results. The heat-maps help to trace out the region of ϵ and v corresponding to the optimum transport in the system. Panel (a) shows that for small ρ , current is maximum for strongest repulsion $\epsilon = 1$, while panel (b) shows that for large ρ a positive $\epsilon < 1$ optimizes the transport. Note however, the scales chosen for left and right panels show that the magnitude of the optimum current is much larger when ρ is large. Mean-field results work reasonably well for large ρ , but fail to capture the optimum transport regime for small ρ .

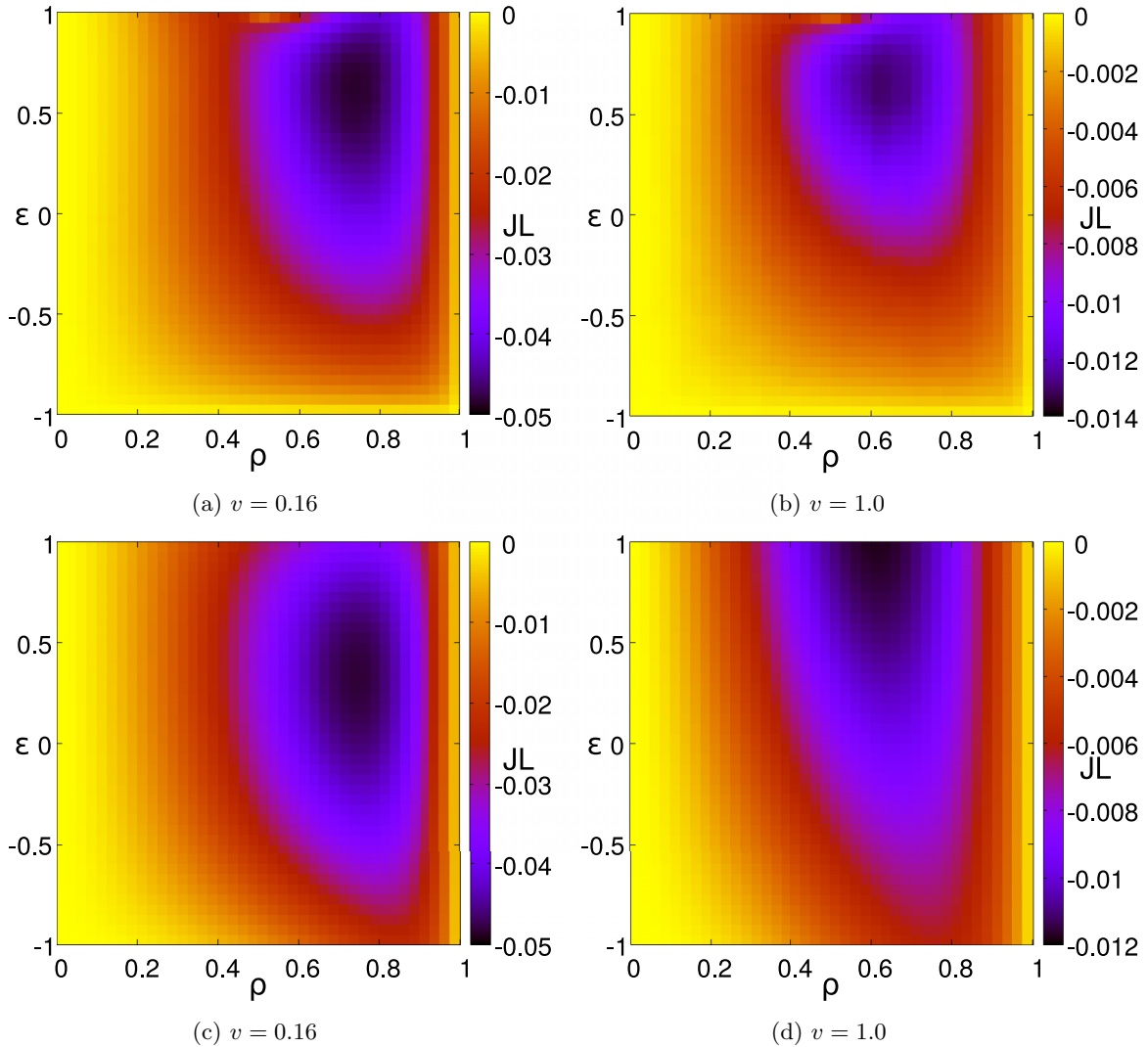


FIG. 7. Numerical results for particle current JL is plotted against ϵ and ρ in panels (a) and (b) while mean-field results are represented in panels (c) and (d). The heat-maps trace out the optimum region for particle current in ϵ - ρ plane. The region corresponds to large ρ and a high positive ϵ . Magnitude of optimum current is higher in left panels where intermediate v value is used.

actual value of maximum current is much higher for $v = 0.16$ as compared to $v = 1$.

IV. NONZERO BULK-HOPPING RATE: $q \neq 0$

In the previous section, we considered the case when the only possible transition in the system is particle hopping out of the defect site. In the present section we consider $q \neq 0$, which allows for movement of particles in the bulk of the system. We are interested to find out how the bulk dynamics affects the current. As expected, for small q , our results are quite similar to what we had presented in the previous section. As q becomes moderate, the presence of bulk diffusion significantly affects the current. We argue below that the bulk dynamics is expected to make a positive contribution to the current. Since the density profile remains homogeneous at sites far away from the defect site, the nonvanishing contribution to the particle current comes from the dynamics around the defect site. For moderate q values, a significant amount of diffusive current flows between the site with density ρ_-

and its left neighbor with density ρ . Since $\rho_- < \rho$, this current will be in the positive direction. Therefore, the presence of the bulk dynamics must add a positive component to the overall particle current. We do not have a mean-field theory for this case to support the numerical data. In the studies below, we consider, for simplicity, only the small and moderate q values.

In Fig. 8, we plot scaled particle current JL vs ϵ for a fixed v and different ρ values. For small bulk diffusion, say, for $q = 0.1$, the behavior is very similar to the trend observed in Fig. 3. As q increases, the contribution from the positive diffusive component in JL becomes enhanced as explained above. For a moderate q value, when the particle density is small, the diffusive current, that principally arises due to the nonhomogeneous density profile about the defect site, dominates over the defect-induced current, resulting in a net current that shows a positive peak at a high value of ϵ . However, for large particle densities, since JL has large negative values for $q = 0$, it remains negative even when q becomes moderately large, although its magnitude decreases because of larger positive contribution coming from bulk dynamics.

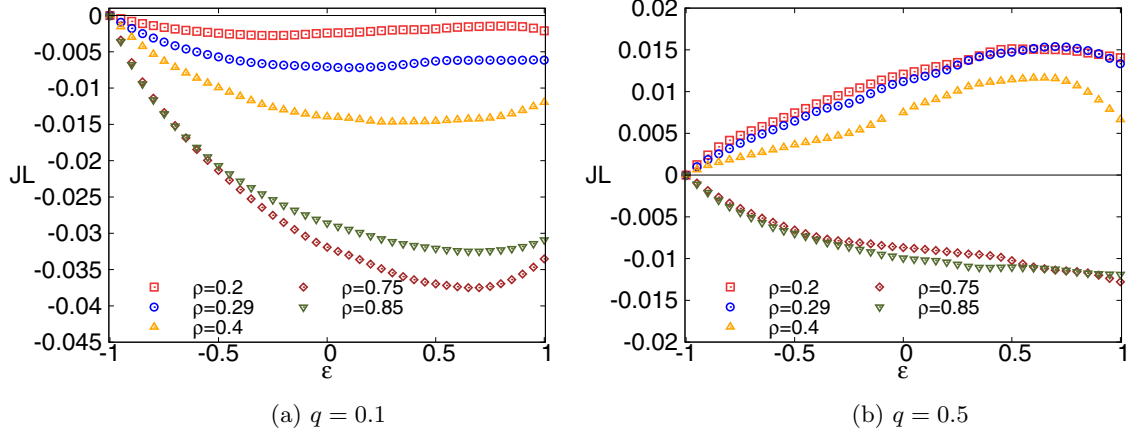


FIG. 8. Scaled current JL is plotted against epsilon for several ρ and two different q values. (a) For small q , current is throughout negative and larger in magnitude for repulsive interaction compared to attractive ones. (b) For moderate q , when the density is low, current reverses sign and becomes positive, while for large density it remains negative.

At large densities, the defect induced negative current wins over the diffusive current and the net negative current becomes maximum at the strongest possible repulsive strength. Such dependence of the system current on interaction strength can be observed in Figs. 9 and 10 as well. Figure 9(a) depicts the variation of JL with ρ for small q showing similar qualitative behavior as observed in Fig. 4. But, for larger q , the current reverses its direction [see Fig. 9(b)] as the density increases, showing a positive peak at a small ρ along with a negative maximum at a large ρ . Figure 10 also captures the non-monotonic dependence of magnitude of the current maxima on the interaction strength for small particle density and moderate bulk diffusion, which is consistent with Fig. 8.

To identify the parameter regime for optimal transport, we show the heatmap in Fig. 11. We have four relevant parameters here: ϵ , ρ , v , and q . For $\rho = 0.29$, we show the variation of current in ϵ - v plane for two different q values. For $q = 0.1$, particle current has both positive and negative peaks, i.e., the optimum current can flow in the direction of the defect movement or in the opposite direction. For any v , the current attains its highest value as ϵ assumes a high positive value.

This can be clearly seen from Fig. 11(a). For $q = 0.5$ however, due to the presence of large diffusive current in the system, only positive current is observed and the optimum transport always happens in the direction of defect movement as observed in Fig. 11(b). The heatmaps also highlight the fact that the positive peaks for any q occur at $\epsilon < 1$, consistent with Fig. 8.

V. SUMMARY AND CONCLUDING REMARKS

In this paper, we have studied Ising-like lattice gases with nearest-neighbor interactions, where the system is driven by a localized (delta) potential barrier, referred to as a “defect,” moving on a ring. We find that the interparticle interaction is crucial in controlling the particle transport in the system: in the presence of an attractive interaction, the time-averaged dc current decreases, whereas a repulsive interaction enhances the current quite significantly, thus resulting in a rich interaction-dominated regime of particle transport in the system and consequently current reversal on tuning various parameters such as the bulk density, defect velocity and interaction strength. The precise mechanism behind the

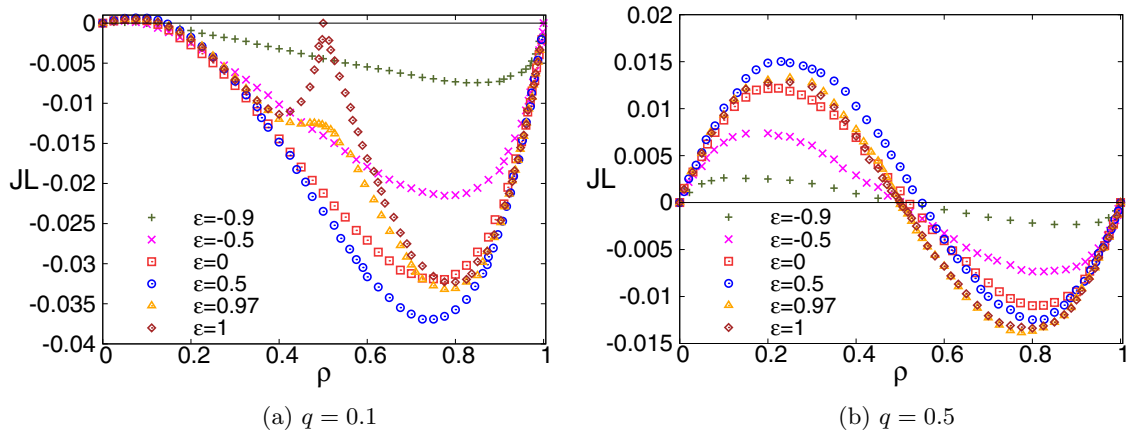


FIG. 9. Variation of scaled current JL with density ρ is shown for different ϵ and two q values. For small q , current shows similar behavior as in $q = 0$ case both for attractive and repulsive interaction. For moderate q , current shows a positive peak at small density and a negative peak at large density. For $\epsilon = 1$ current crosses zero exactly at $\rho = 0.5$.

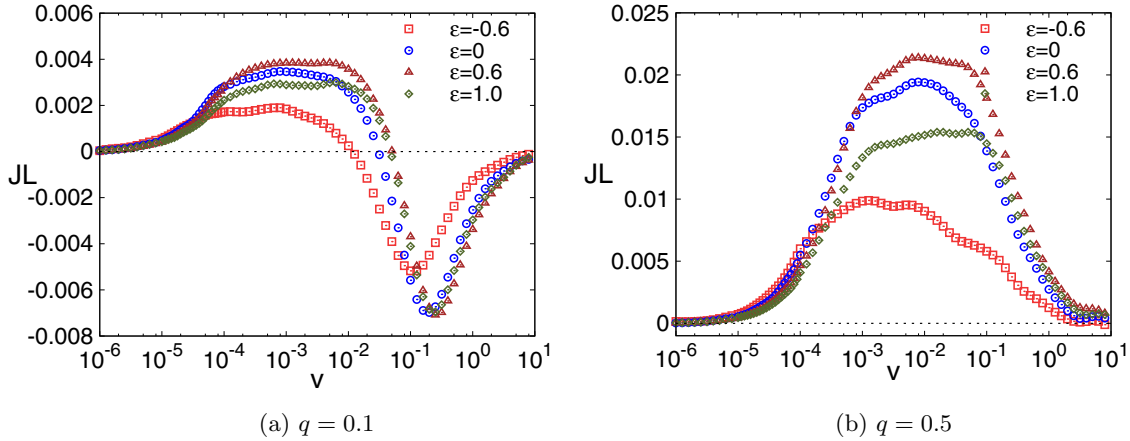


FIG. 10. Scaled current JL is plotted against defect velocity v for different ϵ . For small q current remains almost flat at small v and reverses its direction at an intermediate v , while for moderate q it remains positive throughout for all ϵ .

characteristics of the dc particle current can be understood physically as explained below. The moving potential barrier (defect) creates a traveling density inhomogeneity, which generates a current in the negative direction, i.e., in the direction opposite to the barrier movement, whereas the bulk diffusion generates a current in the direction along the barrier movement. As a result, when the bulk hopping (diffusion) rate vanishes, i.e., when $q = 0$, the particle current is always negative and shows a negative peak as the barrier velocity v and bulk density ρ are varied. Quite remarkably, the negative peak in the current is further enhanced when a strong repulsive interaction is present among the particles. On the other hand, for the nonzero bulk hopping rate $q \neq 0$, as the barrier speed v , bulk density ρ and interaction strength ϵ are varied, the particle current shows both positive and negative peaks, which are in fact due to the competition between the positive contribution from the bulk diffusion and the negative contribution from the barrier movement; however, the extent

of variation is weaker in this case compared to that for $q = 0$. We have been able to identify the precise parameter regime for an optimum transport, which indeed maximizes the magnitude of the particle current. In the case of attractive interaction, a particle prefers to have its nearest neighbor occupied, giving rise to particle clustering. The contribution in the current from the transitions which cause fragmentation of the clusters decreases as the strength of attractive interaction increases, thus resulting in a decreased current. Indeed, unlike repulsive interaction, the current decreases monotonically with the attractive interaction strength, irrespective of defect speed, particle density, and bulk diffusivity. To theoretically understand the above results, we perform a modified mean-field calculation, which—for repulsive interaction, high particle density and negligible bulk diffusion—agrees reasonably well with simulations. Strong attractive interaction causes particle clustering, leading to strong spatial correlations in the system, and the mean-field theory in that case does not work

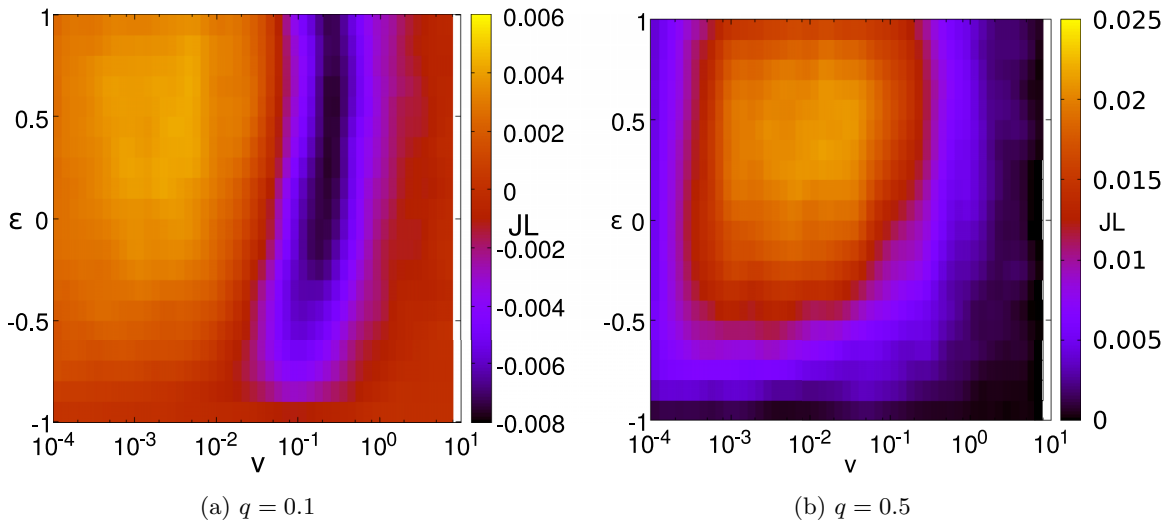


FIG. 11. Numerical results for scaled current JL is plotted against ϵ and v at $\rho = 0.29$. For small q , a positive and a negative peak in the variation of current can be observed from panel (a) while panel (b) shows that there exists a single positive peak in its variation. Such peaks occur at large positive ϵ and at moderate v .

well. Also, for large bulk diffusion, our mean-field theory does not show satisfactory agreement with simulations, again due to the built up of quite strong spatial correlations in the system.

The role of interparticle interactions in controlling particle transport in the presence of a time-dependent drive can be tested in experiments. A periodic potential energy landscape can be created by superimposing external rotating magnetic field on local periodic arrangement of micromagnets [37]. With the help of this periodic potential, micron-size super paramagnetic beads can be separated from a complex mixture by transporting the beads across a substrate. Then, by tuning the rotational frequency of the external field, the mobility of a specific type of beads can be significantly reduced. The interaction among the paramagnetic colloidal particles can be directly tuned using a modulated ratchet potential [38]. In a system of paramagnetic particles dispersed in water, driven across a striped patterned magnetic garnet film, an external rotating magnetic field induces a periodic potential energy landscape and causes directed motion of the particles. Interestingly, by varying the ellipticity of the rotating magnetic field, the interparticle interaction can be changed from attractive to repulsive. Our conclusions can be tested in this kind of a setup.

Throughout this work, we have considered interacting many-particle systems, albeit only on a lattice, where particles hop in discrete steps. Indeed it would be quite interesting to investigate particle transport in a continuum. In the past, there has been some progress made in this direction where the directed particle transport in continuum was found to be crucially dependent on the precise nature of the protocols concerning the externally applied drive. For example, in a system of particles with nearest-neighbor interaction and diffusing on a one-dimensional ring [39], a sinusoidally varying traveling wave potential was found to generate a current always in the direction of the traveling wave itself. However, in a previous work by two of us, it was demonstrated, using numerical simulations, that a moving potential barrier can in fact generate current in either direction, depending on whether the external potential moves uniformly or in discrete jumps [40]. Interestingly, some recent studies have reported multiple current reversal for Brownian particles in the presence of a traveling wave potential [41–43]. In a slightly different context, authors in Ref. [44] numerically investigated the effect of interaction on particle transport in asymmetric channels and observed that, depending on the frequency of the external periodic drive, it is possible to enhance transport by tuning the interaction potential. For single-file diffusion of colloidal particles in an external time-varying force field, various types of interactions such as Weeks-Chandler-Andersen, Yukawa, and super paramagnetic potentials were considered [45], and anomalous transport was observed. Indeed, theoretical understanding of transport in continuum, with such realistic potentials and in the presence of a time-dependent drive, will be of significant interest in the context of obtaining the most efficient directed flow. However, it is worth mentioning that any analytical calculations in such a many-particle continuum model is quite challenging. In this scenario, theoretical studies of lattice models such as those presented here are quite relevant and useful, particularly in terms of analytically

calculating the transport properties, and could initiate further research in this direction.

APPENDIX A: EXPRESSION FOR $W^{(\alpha+1)}$

The (i, j) -th element of the transition matrix [31] can be readily written as

$$\begin{aligned} W_{ij}^{(\alpha+1)} &= 1 - a_+ - a_- & \text{for } i = j = \alpha + 1 \\ W_{ij}^{(\alpha+1)} &= a_- & \text{for } i = j + 1 = \alpha + 1 \\ W_{ij}^{(\alpha+1)} &= a_+ & \text{for } i = j - 1 = \alpha + 1 \\ W_{ij}^{(\alpha+1)} &= 1 & \text{for } i = j \neq \alpha + 1 \\ W_{ij}^{(\alpha+1)} &= 0 & \text{for } i \neq \alpha + 1, i \neq j. \end{aligned} \quad (\text{A1})$$

Here a_{\pm} are the conditional probabilities that, given the defect site is occupied, a particle from the defect site moves to its unoccupied right (left) neighboring site during the residence time τ . For example, when $\alpha + 1 = 1$ and 2, the respective transition matrices can be simply written as

$$\begin{aligned} W^{(1)} &= \begin{bmatrix} 1 - a_+ - a_- & a_+ & 0 & \dots & 0 & a_- \\ 0 & 1 & 0 & 0 & \dots & 0 \\ \dots & \dots & \dots & \dots & \dots & \dots \\ 0 & \dots & 0 & 0 & 1 & 0 \\ 0 & 0 & \dots & 0 & 0 & 1 \end{bmatrix} \\ W^{(2)} &= \begin{bmatrix} 1 & 0 & 0 & \dots & 0 & 0 \\ a_- & (1 - a_+ - a_-) & a_+ & 0 & \dots & 0 \\ 0 & 0 & 1 & 0 & \dots & 0 \\ \dots & \dots & \dots & \dots & \dots & \dots \\ 0 & \dots & 0 & 0 & 1 & 0 \\ 0 & 0 & \dots & 0 & 0 & 1 \end{bmatrix}. \end{aligned} \quad (\text{A2})$$

APPENDIX B: CALCULATION OF a_{\pm} FOR $q = 0$

In the main text, $a_+(a_-)$ is defined as the conditional probability that given the defect site is occupied, a particle hops from the defect site to its empty right (left) neighbor site during the residence time τ of the defect at a single site. Equation (5) provides a formal mathematical definition for a_{\pm} . In this Appendix we outline the calculation for ω_i^{\pm} with $i = 1, 2, \dots, 6$ as explicit functions of ϵ and v .

Let $\hat{1}$ ($\hat{0}$) denote an occupied (empty) defect site. When a particle hops rightward from the defect site, there are six possible local configurations, which are $00\hat{1}01$, $10\hat{1}01$, $00\hat{1}00$, $10\hat{1}00$, $1\hat{1}00$, and $1\hat{1}01$. We number them as $i = 1, 2, \dots, 6$. Similarly, for leftward hopping possibilities are $10\hat{1}00$, $10\hat{1}01$, $00\hat{1}00$, $00\hat{1}01$, $00\hat{1}1$, and $10\hat{1}1$. For a system of size L we divide one Monte Carlo step in L time intervals of length $dt = 1/L$, where $L \gg 1$. For a specific local configuration i , ω_i^+ (ω_i^-) is defined as the probability that a particle hops from the defect site to its right (left) neighboring site during τ . The configurations are numbered in such a way, that $\omega_i^+ = \omega_i^- = \omega_i$. Below we discuss only the rightward hopping

events, which can be easily generalized for leftward hopping as well.

1. Calculation for $\omega_1 = \omega(00\hat{1}01)$

For the local configuration $00\hat{1}01$ the probability that the particle hopping event takes place during the first infinitesimal time step dt is given by $(1 - \epsilon)dt/4$ (see Fig. 1). Probability that no hopping takes place in this interval is

$$\left[1 - \frac{dt(1 - \epsilon)}{4} - \frac{dt}{4}\right] \quad (\text{B1})$$

which includes the possibilities both leftward and rightward hopping attempts was unsuccessful. The probability that the hopping event takes place after time $2dt$ is therefore,

$$\left[1 - \frac{dt(1 - \epsilon)}{4} - \frac{dt}{4}\right] \left[\frac{(1 - \epsilon)dt}{4}\right]. \quad (\text{B2})$$

Similarly the probability that it takes place at time $3dt$ is

$$\left[1 - \frac{dt(1 - \epsilon)}{4} - \frac{dt}{4}\right]^2 \left[\frac{(1 - \epsilon)dt}{4}\right] \quad (\text{B3})$$

and so on. So the probability ω_1 that the hopping happens in any of the τ/dt time steps is

$$\begin{aligned} & \frac{(1 - \epsilon)dt}{4} \left\{ 1 + \left[1 - \frac{(2 - \epsilon)dt}{4}\right] + \left[1 - \frac{(2 - \epsilon)dt}{4}\right]^2 \right. \\ & \quad \left. + \dots + \left[1 - \frac{(2 - \epsilon)dt}{4}\right]^{(\tau/dt)-1} \right\} \\ & = \frac{(1 - \epsilon)dt}{4} \left\{ \frac{1 - [1 - (2 - \epsilon)dt/4]^{\tau/dt}}{1 - [1 - (2 - \epsilon)dt/4]} \right\} \\ & = \frac{1 - \epsilon}{2 - \epsilon} \left[1 - e^{-(2 - \epsilon)/4v}\right] \end{aligned} \quad (\text{B4})$$

where we have used $\tau = 1/v$ and $dt \rightarrow 0$.

2. Results for remaining ω

Following similar steps as outlined above, expressions for all other ω can be derived. We directly present the final results here

$$\begin{aligned} \omega_2 &= \omega(10\hat{1}01) = \frac{1}{2}[1 - e^{-(1 - \epsilon)/2v}] \\ \omega_3 &= \omega(00\hat{1}00) = \frac{1}{2}(1 - e^{-1/2v}) \\ \omega_4 &= \omega(10\hat{1}00) = \frac{1}{2 - \epsilon}[1 - e^{-(2 - \epsilon)/4v}] \\ \omega_5 &= \omega(1\hat{1}00) = [1 - e^{-(1 + \epsilon)/4v}] \\ \omega_6 &= \omega(1\hat{1}01) = (1 - e^{-1/4v}). \end{aligned} \quad (\text{B5})$$

3. Expressions for \mathcal{C}_i^\pm

We provide the formal definitions for \mathcal{C}_i^\pm below. These denote the conditional probability of a specific local configuration, given that the defect site is occupied.

$$\mathcal{C}_1^+ = \text{P}(00\hat{1}01|\hat{1}) = \frac{\langle (1 - \eta_{\alpha-1}^{(\alpha)})(1 - \eta_{\alpha}^{(\alpha)})\eta_{\alpha+1}^{(\alpha)}(1 - \eta_{\alpha+2}^{(\alpha)})\eta_{\alpha+3}^{(\alpha)} \rangle}{\langle \eta_{\alpha+1}^{(\alpha)} \rangle}, \quad (\text{B6})$$

$$\mathcal{C}_2^+ = \text{P}(10\hat{1}01|\hat{1}) = \frac{\langle \eta_{\alpha-1}^{(\alpha)}[1 - \eta_{\alpha}^{(\alpha)}]\eta_{\alpha+1}^{(\alpha)}[1 - \eta_{\alpha+2}^{(\alpha)}]\eta_{\alpha+3}^{(\alpha)} \rangle}{\langle \eta_{\alpha+1}^{(\alpha)} \rangle}, \quad (\text{B7})$$

$$\mathcal{C}_3^+ = \text{P}(00\hat{1}00|\hat{1}) = \frac{\langle [1 - \eta_{\alpha-1}^{(\alpha)}][1 - \eta_{\alpha}^{(\alpha)}]\eta_{\alpha+1}^{(\alpha)}[1 - \eta_{\alpha+2}^{(\alpha)}][1 - \eta_{\alpha+3}^{(\alpha)}] \rangle}{\langle \eta_{\alpha+1}^{(\alpha)} \rangle}, \quad (\text{B8})$$

$$\mathcal{C}_4^+ = \text{P}(10\hat{1}00|\hat{1}) = \frac{\langle \eta_{\alpha-1}^{(\alpha)}[1 - \eta_{\alpha}^{(\alpha)}]\eta_{\alpha+1}^{(\alpha)}[1 - \eta_{\alpha+2}^{(\alpha)}][1 - \eta_{\alpha+3}^{(\alpha)}] \rangle}{\langle \eta_{\alpha+1}^{(\alpha)} \rangle}, \quad (\text{B9})$$

$$\mathcal{C}_5^+ = \text{P}(1\hat{1}00|\hat{1}) = \frac{\langle \eta_{\alpha}^{(\alpha)}\eta_{\alpha+1}^{(\alpha)}[1 - \eta_{\alpha+2}^{(\alpha)}][1 - \eta_{\alpha+3}^{(\alpha)}] \rangle}{\langle \eta_{\alpha+1}^{(\alpha)} \rangle}, \quad (\text{B10})$$

$$\mathcal{C}_6^+ = \text{P}(1\hat{1}01|\hat{1}) = \frac{\langle \eta_{\alpha}^{(\alpha)}\eta_{\alpha+1}^{(\alpha)}[1 - \eta_{\alpha+2}^{(\alpha)}]\eta_{\alpha+3}^{(\alpha)} \rangle}{\langle \eta_{\alpha+1}^{(\alpha)} \rangle}, \quad (\text{B11})$$

$$\mathcal{C}_1^- = \text{P}(10\hat{1}00|\hat{1}) = \frac{\langle \eta_{\alpha-1}^{(\alpha)}[1 - \eta_{\alpha}^{(\alpha)}]\eta_{\alpha+1}^{(\alpha)}[1 - \eta_{\alpha+2}^{(\alpha)}][1 - \eta_{\alpha+3}^{(\alpha)}] \rangle}{\langle \eta_{\alpha+1}^{(\alpha)} \rangle}, \quad (\text{B12})$$

$$\mathcal{C}_2^- = \text{P}(10\hat{1}01|\hat{1}) = \frac{\langle \eta_{\alpha-1}^{(\alpha)}[1 - \eta_{\alpha}^{(\alpha)}]\eta_{\alpha+1}^{(\alpha)}[1 - \eta_{\alpha+2}^{(\alpha)}]\eta_{\alpha+3}^{(\alpha)} \rangle}{\langle \eta_{\alpha+1}^{(\alpha)} \rangle}, \quad (\text{B13})$$

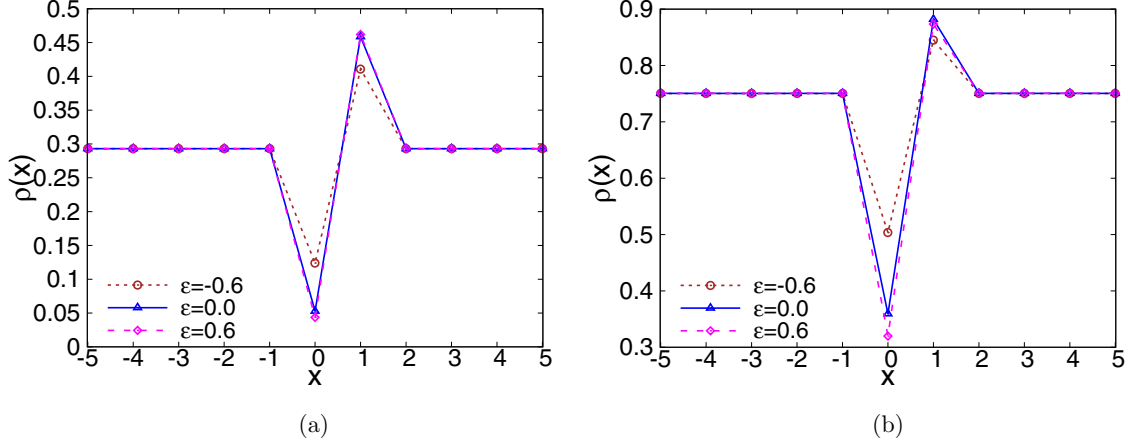


FIG. 12. Panels (a) and (b) show particle density profile $\rho(x)$ for $\rho = 0.29$ and 0.75 , respectively, where x denotes the distance from the defect site. For all bulk density and interaction strength the defect site has a density trough and its right neighbor has a peak. For attractive interaction the trough and peak are relatively shallower.

$$C_3^- = P(00\hat{1}00|\hat{1}) = \frac{\langle [1 - \eta_{\alpha-1}^{(\alpha)}][1 - \eta_{\alpha}^{(\alpha)}]\eta_{\alpha+1}^{(\alpha)}[1 - \eta_{\alpha+2}^{(\alpha)}][1 - \eta_{\alpha+3}^{(\alpha)}] \rangle}{\langle \eta_{\alpha+1}^{(\alpha)} \rangle}, \quad (\text{B14})$$

$$C_4^- = P(00\hat{1}01|\hat{1}) = \frac{\langle [1 - \eta_{\alpha-1}^{(\alpha)}][1 - \eta_{\alpha}^{(\alpha)}]\eta_{\alpha+1}^{(\alpha)}[1 - \eta_{\alpha+2}^{(\alpha)}]\eta_{\alpha+3}^{(\alpha)} \rangle}{\langle \eta_{\alpha+1}^{(\alpha)} \rangle}, \quad (\text{B15})$$

$$C_5^- = P(00\hat{1}1|\hat{1}) = \frac{\langle [1 - \eta_{\alpha-1}^{(\alpha)}][1 - \eta_{\alpha}^{(\alpha)}]\eta_{\alpha+1}^{(\alpha)}\eta_{\alpha+2}^{(\alpha)} \rangle}{\langle \eta_{\alpha+1}^{(\alpha)} \rangle}, \quad (\text{B16})$$

$$C_6^- = P(10\hat{1}1|\hat{1}) = \frac{\langle \eta_{\alpha-1}^{(\alpha)}[1 - \eta_{\alpha}^{(\alpha)}]\eta_{\alpha+1}^{(\alpha)}\eta_{\alpha+2}^{(\alpha)} \rangle}{\langle \eta_{\alpha+1}^{(\alpha)} \rangle}, \quad (\text{B17})$$

APPENDIX C: ADDITIONAL NUMERICAL RESULTS

We have included the plots of local density $\rho(x)$, obtained from simulations, as a function of position x [Figs. 12(a) and 12(b)] for $\rho = 0.29, 0.75$ and $q = 0$. x is measured from the defect site.

We observe that, the density peak and trough are more pronounced in the case of repulsive interaction. We also find that at low density, the difference between the height of the peak and the depth of the trough are small, which justifies the small magnitude of current at low density.

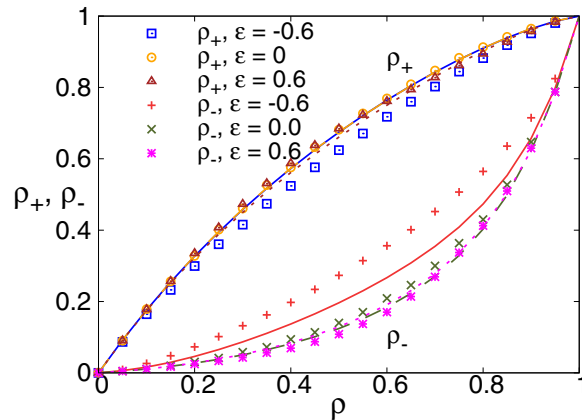


FIG. 13. ρ_{\pm} are plotted against bulk density ρ . Mean-field results are presented by solid ($\epsilon = -0.6$), dashed ($\epsilon = 0$) and dotted ($\epsilon = 0.6$) lines. ρ_+ shows a weaker dependence on ρ compared to ρ_- . For attractive interaction ρ_+ (ρ_-) is noticeably smaller (greater) than that for the hardcore and repulsive interactions. Mean-field results show good agreement for $\epsilon \geq 0$ but for $\epsilon < 0$ quantitative deviation from numerical data is observed. Points, simulations; lines, mean-field theory.

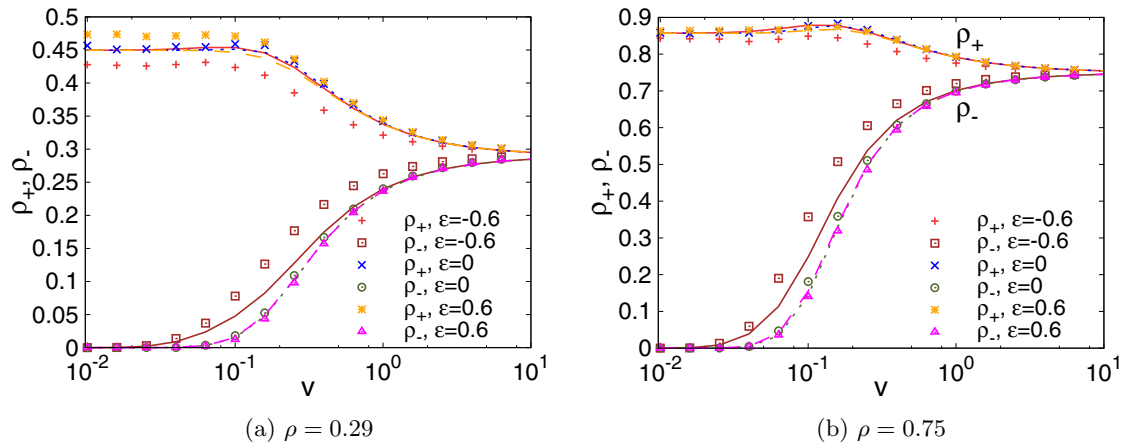


FIG. 14. ρ_{\pm} are plotted against defect velocity v . Mean-field results are presented by solid ($\epsilon = -0.6$), dotted ($\epsilon = 0$), and dashed ($\epsilon = 0.6$) lines which qualitatively capture the variation. For large v both these quantities approach ρ while for small v they show weak variation. Comparing the data for different ϵ values show that for all v repulsive interaction causes highest (lowest) ρ_+ (ρ_-).

We have shown the variation of the peak and trough densities ρ_+ and ρ_- , respectively, as a function of bulk density ρ in Fig. 13, and compare the simulation results (points) to that obtained from the mean-field theory (solid and dashed lines). We find that the variation of ρ_- with ρ is much stronger compared to that of ρ_+ . Such a behavior is also supported by the mean-field theory (lines).

We have studied also the variation of ρ_{\pm} with v for two different ρ (Fig. 14). For small v a particle can almost always hop out of the defect site but as v increases such a transition may not always be possible because of short residence time of the defect [31,32]. Therefore ρ_- (ρ_+) increases (decreases) with v , finally saturating to ρ for very large v . As ϵ increases from negative to positive values, for all v , ρ_- becomes systematically lower and ρ_+ becomes higher, consistent with what we have shown in Fig. 13.

-
- [1] A. Simon and A. Libchaber, *Phys. Rev. Lett.* **68**, 3375 (1992); L. P. Faucheux, G. Stolovitzky, and A. Libchaber, *Phys. Rev. E* **51**, 5239 (1995).
- [2] A. Ashkin, *Phys. Rev. Lett.* **24**, 156 (1970); A. Ashkin, J. M. Dziedzic, J. E. Bjorkholm, and S. Chu, *Opt. Lett.* **11**, 288 (1986).
- [3] J. Berner, B. Müller, J. R. Gomez-Solano *et al.*, *Nat. Commun.* **9**, 999 (2018).
- [4] T. Brazda, C. Julia, and C. Bechinger, *Soft Matter* **13**, 4024 (2017).
- [5] T. Bohlein and C. Bechinger, *Phys. Rev. Lett.* **109**, 058301 (2012).
- [6] J. R. Gomez-Solano, A. Petrosyan, S. Ciliberto, R. Chetrite, and K. Gawedzki, *Phys. Rev. Lett.* **103**, 040601 (2009).
- [7] J. R. Gomez-Solano, L. Bellon, A. Petrosyan, and S. Ciliberto, *Europhys. Lett.* **89**, 60003 (2010).
- [8] V. Blickle, T. Speck, C. Lutz, U. Seifert, and C. Bechinger, *Phys. Rev. Lett.* **98**, 210601 (2007).
- [9] G. M. Wang, E. M. Sevick, E. Mittag, D. J. Searles, and D. J. Evans, *Phys. Rev. Lett.* **89**, 050601 (2002).
- [10] P. Hänggi and P. Marchesoni, *Rev. Mod. Phys.* **81**, 387 (2009).
- [11] A. Terray, J. Oakey, and D. W. M. Marr, *Science* **296**, 1841 (2002).
- [12] F. Penna and P. Tarazona, *J. Chem. Phys.* **119**, 1766 (2003).
- [13] P. Tarazona and U. M. B. Marconi, *J. Chem. Phys.* **128**, 164704 (2008).
- [14] S. Rahav, J. Horowitz, and C. Jarzynski, *Phys. Rev. Lett.* **101**, 140602 (2008).
- [15] S. K. Watson, R. M. Potok, C. M. Marcus, and V. Umansky, *Phys. Rev. Lett.* **91**, 258301 (2003).
- [16] R. D. Astumian, *Phys. Rev. Lett.* **91**, 118102 (2003); R. D. Astumian and P. Hanggi, *Phys. Today* **55**(11), 33 (2002).
- [17] R. Marathe, A. M. Jayannavar, and A. Dhar, *Phys. Rev. E* **75**, 030103(R) (2007).
- [18] P. Reimann, *Phys. Rep.* **361**, 57 (2002).
- [19] N. Golubeva and A. Imparato, *Phys. Rev. Lett.* **109**, 190602 (2012).
- [20] R. Bartussek, P. Hanggi, and J. G. Kissner, *Europhys. Lett.* **28**, 459 (1994).
- [21] T. M. Squires and S. R. Quake, *Rev. Mod. Phys.* **77**, 977 (2005).
- [22] G. A. Cecchi and M. O. Magnasco, *Phys. Rev. Lett.* **76**, 1968 (1996).
- [23] R. Eichhorn, P. Reimann, and P. Hanggi, *Phys. Rev. Lett.* **88**, 190601 (2002).
- [24] L. Machura, M. Kostur, P. Talkner, J. Luczka, and P. Hanggi, *Phys. Rev. Lett.* **98**, 040601 (2007).
- [25] A. K. Chatterjee, U. Basu, and P. K. Mohanty, *Phys. Rev. E* **97**, 052137 (2018).
- [26] Cs. Sándor, A. Libál, C. Reichhardt, and C. J. Olson Reichhardt, *Phys. Rev. E* **95**, 012607 (2017).
- [27] K. Jain, R. Marathe, A. Chaudhuri, and A. Dhar, *Phys. Rev. Lett.* **99**, 190601 (2007).

- [28] R. Marathe, K. Jain, and A. Dhar, *J. Stat. Mech.* (2008) P11014.
- [29] D. Chaudhuri and A. Dhar, *Europhys. Lett.* **94**, 30006 (2011).
- [30] I. Liggett, *Interacting Particle Systems* (Springer-Verlag, Berlin, 1985).
- [31] R. Chatterjee, S. Chatterjee, P. Pradhan, and S. S. Manna, *Phys. Rev. E* **89**, 022138 (2014).
- [32] R. Chatterjee, S. Chatterjee, and P. Pradhan, *Phys. Rev. E* **93**, 062124 (2016).
- [33] P. Kalinay, *Phys. Rev. E* **106**, 044126 (2022).
- [34] *Monte Carlo Methods in Statistical Mechanics*, edited by K. Binder (Springer, Berlin, 1979).
- [35] S. Katz, J. L. Lebowitz, and H. Spohn, *J. Stat. Phys.* **34**, 497 (1984).
- [36] J. S. Hager, J. Krug, V. Popkov, and G. M. Schütz, *Phys. Rev. E* **63**, 056110 (2001).
- [37] B. B. Yellen, R. M. Erb, H. S. Son, R. Hewlin, Jr., H. Shang, and G. U. Lee, *Lab Chip* **7**, 1681 (2007).
- [38] A. V. Straube and P. Tierno, *Soft Matter* **10**, 3915 (2014).
- [39] D. Chaudhuri, A. Raju, and A. Dhar, *Phys. Rev. E* **91**, 050103(R) (2015).
- [40] S. Rana, S. Goswami, S. Chatterjee, and P. Pradhan, *Phys. Rev. E* **98**, 052142 (2018).
- [41] R. Chen, C. Wang, and Z. He, *Chaos Solitons Fract.* **126**, 116 (2019).
- [42] R. Chen, X. Ruan, C. Wang, and L. Jiang, *Physica A* **593**, 126929 (2022).
- [43] A. K. Mukhopadhyay and P. Schmelcher, *Appl. Sci.* **10**, 1357 (2020).
- [44] N. Khatri and P. S. Burada, *J. Stat. Mech.* (2021) 073202.
- [45] E. C. Euán-Díaz, S. Herrera-Velarde, V. R. Misko, F. M. Peeters, and R. Castañeda-Priego, *Biophys. Rev. Lett.* **09**, 413 (2014).